



**HAL**  
open science

## The motion of a freely falling chain tip

Jean-Christophe Géminard, Piotr Pieranski, Waldek Tomaszewski

► **To cite this version:**

Jean-Christophe Géminard, Piotr Pieranski, Waldek Tomaszewski. The motion of a freely falling chain tip. American Journal of Physics, 2005, 74 (9), pp.776-783. ensl-00180258

**HAL Id: ensl-00180258**

**<https://ens-lyon.hal.science/ensl-00180258>**

Submitted on 10 Mar 2008

**HAL** is a multi-disciplinary open access archive for the deposit and dissemination of scientific research documents, whether they are published or not. The documents may come from teaching and research institutions in France or abroad, or from public or private research centers.

L'archive ouverte pluridisciplinaire **HAL**, est destinée au dépôt et à la diffusion de documents scientifiques de niveau recherche, publiés ou non, émanant des établissements d'enseignement et de recherche français ou étrangers, des laboratoires publics ou privés.

# The motion of the freely falling chain tip

W. Tomaszewski\* and P. Pieranski†

*Poznan University of Technology, Poland*

J.-C. Geminard‡

*Ecole Normale Supérieure, Lyon, France*

(Dated: revised March 1, 2006)

## Abstract

The dynamics of the tip of the falling chain is analyzed. Results of laboratory experiments are presented and compared with results of numerical simulations. Time dependences of the velocity and the acceleration of the chain tip for a number of different initial conformations of the chain are determined. A simple analytical model of the system is also considered.

## I. INTRODUCTION

The problem of bodies falling in a gravitational field is so old that it is hard to imagine anything new being added to it. However, the development of numerical simulation methods has a means for the analysis of a few interesting cases, that are difficult to analyze analytically. The dynamics of a falling chain is among them.

A detailed and critical review of the history of the “falling chain” problems, in particular of some erroneous approaches to them, has been given recently by Wong and Yasui<sup>1</sup>. In one case consideration is given to a chain initially gathered in a compact heap located on a table and close to its edge. The motion starts when one of the chain ends is brought over the edge. If one assumes that the chain leaves the heap without friction the model becomes tractable analytically. The surprise is that the acceleration of the chain tip is not, as one would expect,  $g$ , but as Sousa and Rodrigues have found  $g/2^2$ . Wong and Yasui confirm the result and rebuke the history of the long lasting erroneous conviction that the acceleration should be equal  $g/3$ . They locate the source of the error and propose a fool-proof Lagrangian approach to the falling chain problems concluding that ”‘Lagrange’s method gives definitive answers with unmatched ease, clarity and elegance’”. They indicate at the same time that the method of Sousa and Rodrigues is not reliable since it provides an erroneous solution for the falling folded chain.

In the variation of the falling chain problem considered here, the chain is initially attached at both ends to a horizontal support. Then, as one of the ends is released, the chain begins to fall. The case in which the horizontal separation  $\Delta x$  between the ends of the chain equals 0, i.e. the chain is tightly folded, has an analytical solution. According to Wong and Yasui, the solution was for the first time presented by Hamel<sup>3</sup> and then repeated by Calkin and March<sup>4</sup>. The analytical result was confirmed both in experimental measurements<sup>4</sup> and numerical simulations<sup>5,6</sup>. We note that Calkin also considered a different variation of the falling chain problem in which the chain was hanging initially over a smooth horizontal peg and then let to slip down one side<sup>7</sup>. This case is not considered in the present work.

Here, we describe results of experiments analogous to those performed by Calkin and March<sup>4</sup>. In the initial conformation the ends of the chain of length  $L$  are located at the same level but their horizontal separation  $\Delta x$  varies in steps. In the experiments performed by Calkin and March the time was recorded for the tension acting on the support of the fixed

end of the chain to reach its maximum value (i.e. the time at which, as they were implicitly assuming, the tip of the chain reaches its lowest position). Moreover, in their study, the largest value of  $\Delta x$  was around  $0.3L$ . In contrast, for the experiments we performed the largest value of  $\Delta x$  was  $0.999L$ , and the experimental set-up that we used allowed us to record the entire shape of the consecutive conformations of the falling chain. Analyzing the recorded conformations, we are able to quantitatively extract data concerning the time dependencies of the velocity and acceleration of the chain tip. Calkin and March compared their experimental results with the analytical solution of the  $\Delta x = 0$  model. It is clear that the model is not valid for large  $\Delta x$ . To overcome this difficulty we formulated the complete equations of motion for the chain and we integrated them numerically, arriving at a quantitative comparison between the experimental and numerical results. As we shall demonstrate, the not-studied-before case in which the initial distance between the ends of the chain is very close to  $L$  (i.e. when the chain is initially stretched to its maximum length) proves to be very interesting since the vertical motion of the chain tip becomes identical with the motion of a freely falling body. In what follows we shall refer to the latter as the "free fall".

## II. THE FALL OF THE TIGHTLY FOLDED CHAIN – ANALYTICAL SOLUTION

To get intuitive insight into what we can expect in the experiments with the falling chain, let us consider first the case  $\Delta x = 0$ . The complete analysis of this case can be found in the paper by Calkin and March<sup>4</sup>, thus we provide below only its essential assumptions and results. The basic assumption is that the conformations explored by the falling chain can be always considered as consisting of two sections: *a*) the falling section of length  $L_a$ , which decreases with time; *b*) the almost motionless section of length  $L_b$ , which increases with time. Such a division of the chain is possible when the initial horizontal separation of the chain ends equals zero and the chain consists of infinitely many, short and thin segments. In this limit the chain can be seen as a tightly folded, perfectly flowing and infinitely thin continuous filament.

Initially both ends of the chain are attached to a point of support  $O$ , the vertical position of which  $y = 0$ . Then, at time  $t = 0$ , one of the ends of the chain is released and the chain begins to fall. Figure 1 presents schematically the geometry of the system. We assume

that the chain has a total length of  $L$  and that its mass,  $M$ , is distributed uniformly along  $L$ . To simplify the final analysis of the results, we introduce a new variable  $h$  describing the distance of the freely falling tip from its initial position. The  $h$ -axis is thus oriented downwards, in the direction of the gravitational field. In what follows, we shall refer to  $h$  as the *fall distance*. By assuming that energy is conserved it can be shown that, the velocity,  $v_c$ , acceleration,  $a_c$ , and time,  $t_c$ , of the chain tip versus the fall distance,  $h$ , are given by the following formula:

$$v_c(h) = \sqrt{\left(1 + \frac{L}{L-h}\right)gh}, \quad (1)$$

$$a_c(h) = \frac{1}{2} \left[ 1 + \left(\frac{L}{L-h}\right)^2 \right] g, \quad (2)$$

$$t_c(h) = \int_0^h \sqrt{\frac{L-s}{gs(2L-s)}} ds. \quad (3)$$

Thus, it can be concluded from analyzing the above equations, that both the velocity and the acceleration of the chain tip diverge at time  $t_c(L)$ , when the tip reaches its lowest position,  $h = L$ . On the other hand, at small  $h$  the velocity and acceleration are approximated with the well known formula describing the dynamics of the free fall:

$$v_b(h) = \sqrt{2gh}, \quad (4)$$

$$a_b(h) = g, \quad (5)$$

$$t_b(h) = \sqrt{2h/g}. \quad (6)$$

As calculated by Calkin and March, time  $t_c(L)$ , at which the tip of the falling folded chain reaches its lowest position, equals

$$t_c(L) = .847213 t_b(L) \quad (7)$$

where  $t_b(L)$  is the time of the free fall. As clearly shown in Figure 5 of their report, the experimentally established time of the chain fall decays with  $\Delta x$  agreeing with the theoretically found value only at  $\Delta x \approx 0.05L$ . In section VI we shall discuss this result in more detail.

### III. LABORATORY EXPERIMENTS

The focus of our experimental study is the dynamics of the falling chain with particular interest in comparing it to the dynamics of a freely falling weight. In order to accentuate the comparison of differences in trajectories for the two cases, we designed an experimental setup that makes it possible to record the simultaneous motions of the two objects.

The ball chain used consists of stainless-steel identical segments which are made from rods and spheres attached to each other, see Figure 2. The total length of a segment  $l = (4.46 \pm 0.01)10^{-3}$  m and the diameter of the spheres are  $\phi = (3.26 \pm 0.01)10^{-3}$  m. In addition, the minimum radius of curvature for which the chain can exist without loading any elastic energy is  $R_{min} = (4.8 \pm 0.2) 10^{-3}$  m. We use a chain of length  $L = 1.022$  m, which corresponds to  $n = 229$  segments for a total mass of  $M = (2.08 \pm 0.01)10^{-2}$  kg.

The chain is tightly attached at one end to a firm support  $O$  by means of a thin thread, see Figure 2. At the other edge located at point  $P = (x_0, y_0)$ , the chain ends with a rod (we open and remove the last sphere) to which we attach a thin nylon cord (fishing line, diameter  $10^{-4}$  m). The free-falling weight, a sinker (a lead weight used for sinking fishing lines) of mass  $\mathcal{M} = 10^{-2}$  kg, is then attached to the other end of the nylon cord (length about 5 cm). We then extend the nylon cord between two nails and a thin metallic wire (nickel, diameter  $10^{-4}$  m) as sketched in Figure 2. The whole system is adjusted so as to insure that the sinker and both ends of the chain are at the same level,  $y = 0$ . The setup can be displaced horizontally in order to choose the initial horizontal separation between the two ends of the chain. As the mass of the sinker  $\mathcal{M}$  is about half the total mass of the chain  $M$ , the system is almost always equilibrated (in addition, mechanical equilibrium is further insured by the solid friction in the contact regions of the nylon wire with the nails and the metallic wire). Thus, the initial conformation formed by the chain after damping of all the disturbances, is close to a catenary curve<sup>16</sup>.

Injecting a large electric current (about 1 A) through the nickel wire results in cutting suddenly the nylon wire at the point where they make contact; the sinker and the end of the chain then simultaneously start to fall freely under the action of gravity. We point out that they both fall with a small piece of nylon cord attached to them. However, as the force that pushes the cord against the nails vanishes, the friction force vanishes as soon as the cord is cut. In addition, during the free fall, the sections of cord have no effect on the dynamics as

the mass of nylon is negligible in comparison to the mass of the sinker or chain.

The falling chain and weight are imaged with a standard CCD video camera (Panasonic WV-BP550/G) and the images are recorded on a video cassette recorder. The chosen shutter speed (1/4000 s) is adequate for obtaining clear images of both the chain and sinker (Figure 3). The filmed sequences of events are digitized afterward by means of a Macintosh computer equipped with a frame grabber board (Data Translation DT2255). Further analysis with image-processing software (NIH-Image) makes possible to recover 50 images per second from the movies which are initially made from 25 interlaced images per second. The interlacing allows us to double the time resolution but results in a loss in the spatial resolution, which is typically of about 4 mm per pixel.

The positions of both the falling chain tip and the sinker at consecutive times  $t_i, i = 0, 1, 2, \dots$ , are determined from the digitized images. To simplify our discussion of the results, the experimentally determined positions of the falling objects will be given as the vertical distance  $h$ , and horizontal distance  $w$  which are defined by deviations of their  $x(t)$  and  $y(t)$  coordinates from their initial values  $(x_0, y_0)$ :

$$\begin{aligned} w(t) &= x_0 - x(t), \\ h(t) &= y_0 - y(t), \end{aligned} \tag{8}$$

In what follows we shall refer to the variables as the vertical,  $h$ , and horizontal,  $w$ , fall distances. According to their definitions, in the initial stages of the falling process both of the falling distances are positive. In all experiments  $y_0 = 0$ , while  $x_0$  was varied in four steps from about 1 m to 0.25 m. Note that since the motionless end of the chain is attached to point  $(0, 0)$ , the initial horizontal separation of the chain ends is  $\Delta x = x_0$ . In view of this equality, we denote the initial separation by  $x_0$ . Experimental results are compared to numerical predictions in Section VI.

#### IV. MODEL OF THE FALLING CHAIN AND ITS EQUATIONS OF MOTION

One can define a few discrete models of the chain; below we present one of them. Its equations of motion will be formulated for the case, in which one of the chain ends is attached to the fixed support while the other one is free. Let us note that similar models have been considered before<sup>5,8,9</sup>.

The free end of the chain moves under the action a gravitational field. To simplify the model, we first assume that the chain is constrained to move only in the vertical plane denoted by  $(x, y)$ . The chain has mass  $M$ , length  $L$  and consists of  $n$  thin cylindrical rods (in the following we shall refer to them as segments) with masses  $m_i = m = M/n$ ,  $i = 1..n$ , and lengths  $l_i = l = L/n$ ,  $i = 1..n$ . All the segments are considered to be rigid and cannot be deformed. Consecutive segments are connected by joints with friction. Figure 4 shows the geometric representation of our model.

In order to formulate the equations of motion, generalized coordinates, which rigorously determine the state of the system, must be specified. Following our predecessors<sup>8</sup>, we describe the system using angular coordinates indicating the inclination of the consecutive segments with respect to the horizontal  $x$ -axis.

The position of the first element is determined by the angle  $\varphi_1$ . Similarly, the position of the second element is described by the angle  $\varphi_2$ , etc... The global conformation of the chain in the plane is uniquely expressed by all angles  $\varphi_i$ ,  $i = 1..n$ . The angles are referred to as generalized coordinates of the system.

The Cartesian coordinates of the  $i$ -th mass center  $(x_i, y_i)$  can be written as follows:

$$\begin{aligned} x_i &= \sum_{j=1}^{i-1} l \cos \varphi_j + \frac{1}{2} l \cos \varphi_i, \\ y_i &= \sum_{j=1}^{i-1} l \sin \varphi_j + \frac{1}{2} l \sin \varphi_i. \end{aligned} \tag{9}$$

Using the generalized coordinates we derive the Lagrange equations of motion and begin by considering the energy of the system. The motion of the chain is considered as a combination of translational and rotational motions of its segments. Each segment has a moment of inertia  $I_i = 1/12ml^2$ ,  $i = 1..n$ , calculated around the axis perpendicular to the  $(x, y)$  plane and passing through the center of mass of the segment. Taking into consideration the relations given in Equation (9), the kinetic energy of the chain is given by:

$$T = \frac{1}{2} \sum_{i=1}^n (m (\dot{x}_i^2 + \dot{y}_i^2) + I_i \dot{\varphi}_i^2), \tag{10}$$

where, the dot represents the derivative with respect to the time  $t$ . The potential energy of the  $i$ -th segment is given by  $mgy_i$ , where  $g$  is the gravitational acceleration. Thus, the

potential energy of the chain may be expressed as:

$$U = \sum_{i=1}^n mgy_i. \quad (11)$$

To make our model more general, we introduce damping through Rayleigh dissipation function<sup>10</sup>:

$$\mathcal{R} = \frac{1}{2}r \sum_{i=1}^n (\dot{\varphi}_i - \dot{\varphi}_{i-1})^2, \quad (12)$$

where,  $r$  is the dissipation coefficient. We assume that the joint which connects the first element of the chain to the support is free of dissipation. This is equivalent to the assumption that  $\dot{\varphi}_0 = \dot{\varphi}_1$ . A similar definition of dissipation was used previously<sup>5,9</sup>.

The motion of the falling chain is governed by the system of Lagrange equations of the second kind:

$$\frac{d}{dt} \left( \frac{\partial \mathcal{L}}{\partial \dot{\varphi}_i} \right) - \frac{\partial \mathcal{L}}{\partial \varphi_i} + \frac{\partial \mathcal{R}}{\partial \dot{\varphi}_i} = 0, \quad i = 1..n, \quad (13)$$

where,  $\mathcal{L} = T - U$  is the Lagrangian of the system. Applying (10), (11), (12) and (13) we find the set of  $n$  equations describing the motion of a chain:

$$\sum_{j=1}^n m_{i,j} c_{i,j} \ddot{\varphi}_j = - \sum_{j=1}^n m_{i,j} s_{i,j} \dot{\varphi}_j^2 + \frac{r}{ml^2} (\dot{\varphi}_{i-1} - 2\dot{\varphi}_i + \dot{\varphi}_{i+1}) - \frac{g}{l} a_i c_i, \quad i = 1..n, \quad (14)$$

where,  $c_i = \cos(\varphi_i)$ ,  $c_{i,j} = \cos(\varphi_i - \varphi_j)$ ,  $s_{i,j} = \sin(\varphi_i - \varphi_j)$ ,  $a_i = n - i + \frac{1}{2}$  and  $m_{i,j} = \begin{cases} n - i + \frac{1}{3}, & i = j \\ n - \max(i, j) + \frac{1}{2}, & i \neq j \end{cases}$ .

Section V is dedicated to the results of the numerical solutions of Equation (14).

## V. NUMERICAL EXPERIMENTS

The equations of motion derived in the previous section can be integrated numerically thus allowing us to simulate the motion of the falling chain. In presence of dissipation, the resulting system of equations becomes stiff and requires specific numerical methods. We selected the RADAU5 algorithm by Hairer & Wanner (<http://www.unige.ch/~hairer/software.html>) designed for stiff problems. It is based on the implicit Runge-Kutta scheme of order five with the error estimator of order four<sup>11</sup>.

Numerical simulations were performed to reproduce results of the experiments described in Section III. Thus, as the initial configuration of the chain, we used the discrete catenary curve shown in Figure 2 with four different separations between the ends of the chain: *a*)  $x_0 = 1.019$  m, *b*)  $x_0 = 0.765$  m, *c*)  $x_0 = 0.510$  m and *d*)  $x_0 = 0.255$  m identical to the separations used in the laboratory experiments. These simulations were carried out for a chain with  $n = 229$ ,  $L = 1.02$  m,  $M = 0.0208$  kg,  $g = 9.81$  m/s<sup>2</sup> and time  $t \in [0, 0.5]$  s. The only remaining free parameter was the dissipation parameter  $r$ . As such  $r$  was used to find the best agreement of the numerical results with the laboratory experiments. To compare the numerical results to the experimental data, we monitored the distance between the positions of the chain tip found in the consecutive frames of the video recordings and the positions found in the numerical simulations at the same times. The deviation between laboratory and numerical data obtained in a single experiment is defined as follows:

$$\delta = \sqrt{\frac{1}{N} \sum_{i=1}^N (w_i - \hat{w}_i)^2 + (h_i - \hat{h}_i)^2}, \quad (15)$$

where the  $N$  denotes the number of analyzed frames. Points  $(w_i, h_i)$  and  $(\hat{w}_i, \hat{h}_i)$  for  $i = 1..N$  are here the horizontal and vertical deviation from the initial position of the chain tip found in consecutive frames of the laboratory and numerical experiments, respectively. In order to find the optimal value of  $r$  providing the best fit for all four experiments *a*), *b*), *c*) and *d*) we determined the total distance

$$\Delta = \delta^{(a)} + \delta^{(b)} + \delta^{(c)} + \delta^{(d)}. \quad (16)$$

$\Delta$  depends on the chosen value of  $r$ ; we have investigated its values in the range from  $r_1 = 0$  to  $r_2 = 10^{-4}$  Nms. The optimal value of dissipation parameter, found with the use of a *least-square* algorithm based on the **SVDFIT** procedure<sup>12</sup>, was equal  $r = 2.163 \cdot 10^{-5}$  Nms.  $\Delta(r)$  reaches here its minimum value equal 0.02479 m. At the specified above ends of the analyzed range of  $r$  the deviation parameter  $\Delta(r)$  was equal  $\Delta(r_1) = 0.029845$  m and  $\Delta(r_2) = 0.03357$  m. Table I provides a summary of how well the data for each of the four experimental cases is fit by the optimal value of  $r$ .

Figure 5 provides a further comparison between the numerical simulations and experimental results. Here the time evolution of the vertical,  $h$ , and horizontal,  $w$ , positions of the tip of the falling chain are reported. One clearly sees an excellent agreement between the simulated and experimental data.

The consecutive conformations of the falling chain found in the numerical simulations are presented in Figure 6. These conformations correspond to the same times at which we recorded the laboratory experiments. In addition, positions of the freely falling body are also shown in the figure. As one can see by comparing Figures 3 and 6, the shapes of the experimental and numerical conformations are nearly identical.

## VI. QUANTITATIVE ANALYSIS

Quantitative analysis of the digital images recorded in the laboratory experiments provided us with sets of discrete data representing the vertical,  $h$ , and horizontal,  $w$ , fall distances of the chain tip versus time. Using the data we have found the value of the dissipation parameter at which numerical simulations best fit the experimental data (Table I). As seen in Figure 5 the agreement is very good. Thus, to closely analyze the details of the falling chain dynamics we use the data obtained at small time steps from the numerical simulations.

We begin by analyzing the interesting question concerning the relation between the time dependencies of the vertical fall distances of the chain tip and the falling sinker (Figure 5). It is worth noticing that in case  $a$ ), where the initial conformation of the chain is straight and horizontal, the vertical fall of the chain tip and the falling sinker are identical up to the moment in time at which, having reached its maximum vertical fall distance, the tip starts moving upwards. This observation becomes clear when one notices that during the fall the chain end remains horizontal - its vertical motion must thus be identical with the falling sinker. The chain end remains horizontal because the chain displays no elasticity and no energy is stored in bent regions. This phenomenon, found both in the laboratory experiments and confirmed by the numerical simulations, suggests the existence of an approximate analytical treatment of the problem. However, we have thus far not been able to formulate an analytical solution.

In cases  $b$ ),  $c$ ) and  $d$ ) the vertical fall distance of the chain tip, up to the moment of time  $t_{h_{max}}$  at which the vertical fall distance of the chain tip reaches its maximum value  $h_{max}$ , is seen to be always ahead of the vertical fall distance of the sinker. This observation is sometimes summarized by the general statement, that *the chain falls faster than a body*.

To further understand this we analyze the time dependencies of the velocity  $v_c$  and the acceleration  $a_c$  of the chain tip. In order to do so we have performed a series of numerical

experiments with  $x_0$  in the range of  $[0.1, \dots, 1.02)$  m. All other parameters of the numerical simulation were the same as defined in the previous section. The smallest value of the initial separation  $x_0$  was equal to 0.1 m due to the fact that smaller initial separations produced very complex chain-fall dynamics. This fact was seen in both numerical simulations and laboratory experiments. We also note that, by velocity and acceleration we mean here the moduli of the velocity and acceleration vectors.

Figure 7 presents plots of both the velocity and the acceleration versus time for four initial spacings  $x_0$ . Two characteristic features in these plots are the peak heights and the times at which these maxima occur. In Figure 8a, the dependence of  $v_{max}$  on  $x_0$  and  $v_{h_{max}}$  (i.e. the velocity of the chain tip at its lowest position  $h_{max}$ ) on  $x_0$  is displayed. At small  $x_0$  there exists a short interval within which  $v_{max}$  slightly increases reaching its global maximum at  $x_0 \approx 0.1314$  m. Then, over a broad interval,  $v_{max}$  decreases reaching its global minimum value at  $x_0 \approx 0.9040$  m. Up to this value of  $x_0$ , the velocity  $v_{h_{max}}$  is smaller than the maximum velocity  $v_{max}$ . For  $x_0 > 0.9040$  m, when the maximum extension of the chain is approached, the two velocities become practically equal.

As Figure 9a reveals, the time  $t_{v_{max}}$ , at which the velocity of the chain tip reaches its maximum value, precedes in general the moment of time  $t_{h_{max}}$  at which the chain tip reaches its lowest position  $h_{max}$ . The lowest position of the chain tip is reached fastest for  $x_0 \approx 0.5500$  m (i.e. when the initial horizontal distance between the chain ends is approximately half of its total length), while  $t_{h_{max}}$  is longest when the chain is initially straight. Figure 9a provides also a comparison between the time  $t_{v_{max}}$  of the maximum velocity and the time  $t_c(L)$  of the velocity divergence found in the analytically solvable model presented in Section II. As seen in the figure, the two times are close to each other at the values of  $x_0$  at which  $v_{max}$  reaches its global maximum and minimum. In the whole range of  $x_0$  located between the two values,  $t_{v_{max}}$  is less than  $t_c(L)$ .

Figure 9b provides the relation between the maximum fall distance of the chain tip,  $h_{max}$ , and the fall distance,  $h_{v_{max}}$ , at which the tip reaches its maximum velocity as a function of the initial separation of the chain ends. As before one can clearly see that in general the maximum velocity is reached before the chain tip reaches its maximum fall distance. Let us note that in the whole studied range of  $x_0$  the maximum fall distance never reaches the theoretically possible value  $L$ , although as the plot of  $h_{max}$  vs.  $x_0$  suggests, it tends to it at  $x_0 \rightarrow 0$ .

The last question we have addressed concerning the velocity data is the correlation between the value of the peak velocity,  $v_{max}$ , and the time,  $t_{v_{max}}$ , at which it is reached. As we have demonstrated before, the peak of the velocity is highest at a small initial separation of the chain ends, but one should not draw the conclusion that it is thus reached in the shortest time. As seen in Figure 9a the initial separation of the chain ends at which the velocity peak is reached fastest amounts to about  $x_0 \approx 0.7000$  m.

Figure 7b presents plots of the acceleration of the chain tip versus time for a few values of the initial separation  $x_0$ . As in the case of the velocity plots, we also observe here distinct peaks. Figure 8b demonstrates clearly, that the highest peak in acceleration is observed at the smallest initial separation of the chain end. Its value, at the experimentally studied case of  $x_0 = 0.255$  m, amounts to  $7352 \text{ m/s}^2$ , thus it is about 40 times larger than the value observed at  $x_0 = 0.765$  m, where it equals to  $186.3 \text{ m/s}^2$ . That such large values of the acceleration are realistic was demonstrated by Krehl et. al.<sup>13</sup> who studied the dynamics of the cracking whip. One may ask about the relation between the dynamics of the falling chain and that of the whip<sup>14,15</sup>. At the first sight the two systems seem to be completely different since in the cracking whip problem the gravitational forces are in general neglected. Let us notice, however, that the end of the folded whip attached to the whip handle is subject to a strong acceleration. Changing the laboratory reference frame to the non-inertial frame moving with the end of the handle, we introduce into the system strong inertial forces equivalent to the gravitational ones. Thus, all conclusions to which we arrived considering the falling chain are applicable also in the case of the accelerated whip. In particular, it becomes clear that there exists a special conformation, to which the whip should be brought before its handle starts accelerating, for which the whip tip will eventually reach the maximum, exceeding the speed of sound velocity, thus allowing one to produce the crack sound.

The last question we considered analyzing results of the laboratory and numerical experiment was if the acceleration  $a_{h_{max}}$  which the chain tip reaches at its lowest position  $h_{max}$  is the maximum acceleration  $a_{max}$ . Figure 8b demonstrates that this is not generally the case.

## VII. SUMMARY AND DISCUSSION

The experimental and numerical work here reveals new and interesting facts concerning the dynamics of the falling chain. Let us summarize them.

1. The dependencies of both the velocity and acceleration on time display distinct peaks the height of which depends on the initial separation of the chain ends. The highest peaks are observed for small initial separations. There exists an approximate, analytical description of tightly folded chain dynamics explaining the origin of the rapid increase of the velocity and acceleration. The theory is however unable to predict the finite height of the peaks. (In the analytical model both the velocity and the acceleration diverge.)
2. For our case, the velocity peak is highest at  $x_0 = 0.1288 L$ , whereas its amplitude is smallest for  $x_0 = 0.8863 L$ .
3. Quite fascinating, we find that in the case for which the initial separation of the chain ends is largest, the dynamics of the vertical fall of the chain tip proves to be identical with the dynamics of the free fall. This corresponds with the fact that the end section of the chain remains horizontal during the fall. This observation suggests the existence of an approximate analytical treatment.
4. As a rule, the time at which the chain tip reaches its maximum velocity generally comes before the time at which it reaches its lowest vertical position. Only at the initial separation of the chain ends larger than  $0.8863 L$  we find otherwise.
5. The ratio of the amplitudes of the highest and smallest acceleration peaks is about 166.5, which is unexpectedly large. This may have some practical implications, since at the time when the acceleration reaches its highest value, the force acting on the chain tip also becomes very large and may lead to damage of the chain.

Dynamics of the falling chain hides certainly a few more interesting details. The same, even to a larger extent, concerns the dynamics of the falling rope, since in this case the dissipation plays a much more important role and elasticity becomes a crucial factor.

## Acknowledgment

The authors would like to thank S. Breiter for helpful discussions and V. Bergeron for his critical reading of the manuscript.

---

\* Electronic address: `waltom@phys.put.poznan.pl`

† Electronic address: `pieransk@man.poznan.pl`

‡ Electronic address: `jean-christophe.geminard@ens-lyon.fr`

- <sup>1</sup> Chun Wa Wong and Kosuke Yasui. Falling chains, 2005.
- <sup>2</sup> C. A. de Sousa and V. H. Rodrigues. Mass redistribution in variable mass systems. *Eur. J. Phys.*, 25:41–49, 2004.
- <sup>3</sup> G. Hamel. *Theoretische Mechanik*. Springer–Verlag, second revised edition, 1949.
- <sup>4</sup> M. G. Calkin and R. H. March. The dynamics of a falling chain: I. *American Journal of Physics*, 57:154–157, February 1989.
- <sup>5</sup> M. Schagerl, A. Steindl, W. Steiner, and H. Troger. On the paradox of the free falling folded chain. *Acta Mech.*, 125:155–168, 1997.
- <sup>6</sup> W. Tomaszewski and P. Pieranski. Dynamics of ropes and chains. I. The fall of the folded chain. *New J. Phys.*, 7(45), 2005.
- <sup>7</sup> M. G. Calkin. The dynamics of a falling chain: II, February 1989.
- <sup>8</sup> J. Kommers. Notes on the Physics of Fly Casting Simulation. Technical report, MIT Center of space research, 1995.
- <sup>9</sup> J. Galán, W. B. Fraser, D. J. Acheson, and A. R. Champneys. The parametrically excited upside-down rod: an elastic jointed pendulum model. Technical Report 2001.17, Bristol Center for Applied Nonlinear Mathematics, 2001.
- <sup>10</sup> H. Goldstein. *Classical Mechanics*. Addison–Wesley, 2nd edition, 1980.
- <sup>11</sup> E. Hairer and G. Wanner. *Solving Ordinary Differential Equations II: Stiff and Differential–algebraic Problems*. Springer–Verlag, second revised edition, 1996.
- <sup>12</sup> W. H. Press, B. P. Flannery, S. A. Teukolsky, and W. T. Vetterling. *Numerical recipes in C: The art of scientific computing*. Cambridge University Press, second edition, 1992.
- <sup>13</sup> P. Krehl, S. Engemann, and D. Schwenkel. The puzzle of whip cracking-uncovered by a corre-

lation of whip-tip dynamics with shock wave emission. *Shock Waves*, 8:1–9, 1998.

<sup>14</sup> T. McMillen and A. Goriely. Shape of a Cracking Whip. *Phys. Rev. Lett*, 88(24), 2002.

<sup>15</sup> T. McMillen and A. Goriely. Whip waves. *Physica D*, 184(1-4):192–225, 2003.

<sup>16</sup> A word of caution seems here necessary; from the rigorous point of view the initial conformation formed in the experiments with chains built from a finite number of segments is not a catenary curve. That this is the case one can see immediately considering the conformation of a chain built from an odd number of segments whose ends are fixed to points located at the same level and separated in the horizontal direction by the length of a single segment. In such a case the initial conformation consists of two exactly vertical pieces. This was the conformation used by Schagerl in his laboratory experiments<sup>5</sup>

## Tables

TABLE I: Deviation between experimental and numerical results,  $\delta_r$  for three different values of the dissipation parameter  $r = 0, 2.163 \cdot 10^{-5}$  and  $10^{-4}$  [m].

Experiment:	$\delta_0$ [m]	$\delta_{2.163 \cdot 10^{-5}}$ [m]	$\delta_{10^{-4}}$ [m]
<i>a)</i>	0.008406	0.007672	0.01038
<i>b)</i>	0.006851	0.006654	0.00659
<i>c)</i>	0.006191	0.005912	0.00669
<i>d)</i>	0.008397	0.004552	0.00991

**Figure Captions**

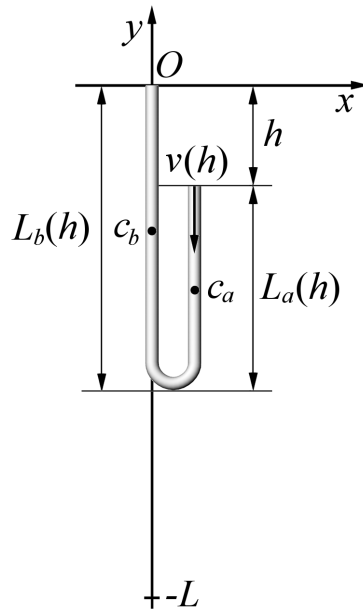


FIG. 1: Geometry of the conformation of the tightly folded chain at time  $t > 0$ . The position of the falling chain is described in terms of  $h$ . Section  $a$ ) of the chain is falling down while section  $b$ ) is motionless;  $c_a$  and  $c_b$  are their centers of mass.

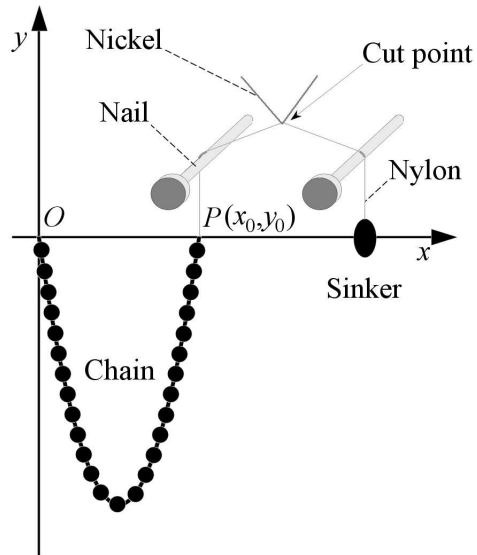


FIG. 2: Schematic of the experimental setup used in this study.

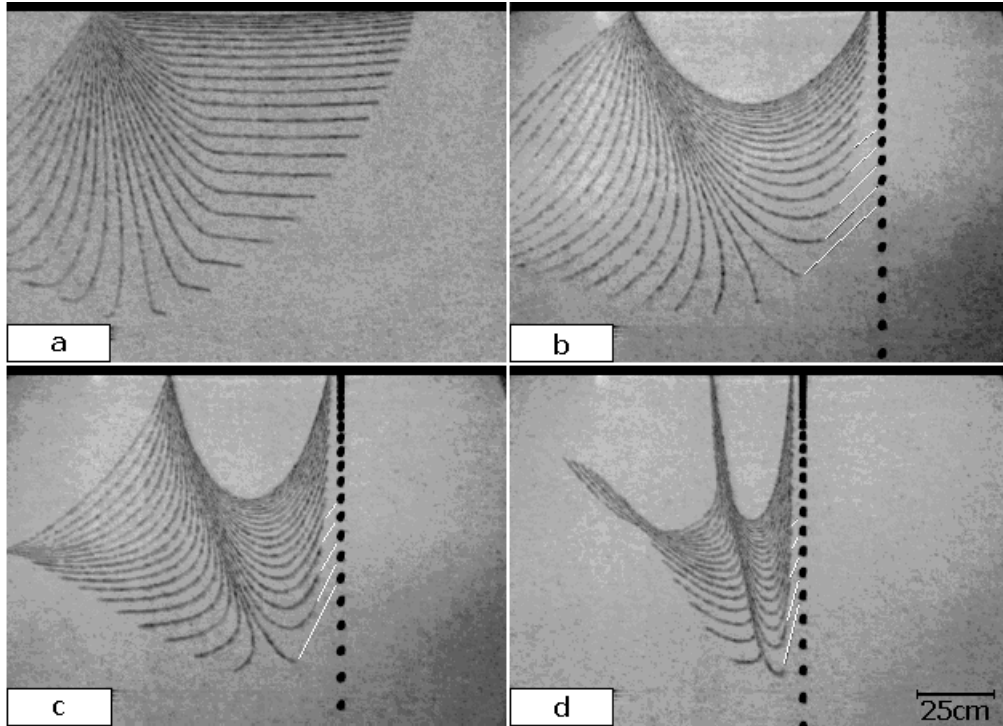


FIG. 3: Successive conformations of the falling chain vs. time. The left end of the chain remains attached to the frame, while the right end is free to fall due to gravity. In *b*), *c*) and *d*), white lines have been sketched into the photographic sequence to connect the free falling end of the chain to the freely falling sinker for the last five images before the maximum extension of the chain (length  $L = 1.022$  m, time spacing between the successive images  $1/50$  s, initial separation between the chain ends: *a*)  $x_0 = 1.019$  m, *b*)  $x_0 = 0.765$  m, *c*)  $x_0 = 0.510$  m, and *d*)  $x_0 = 0.255$  m).

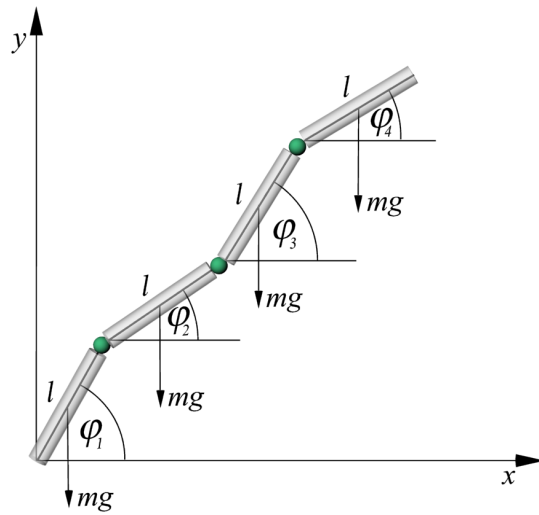


FIG. 4: Schematic representation of the model.  $\varphi_i$  corresponds to the angle of inclination,  $m$  the mass or the chain segment and  $g$  the gravitational acceleration.

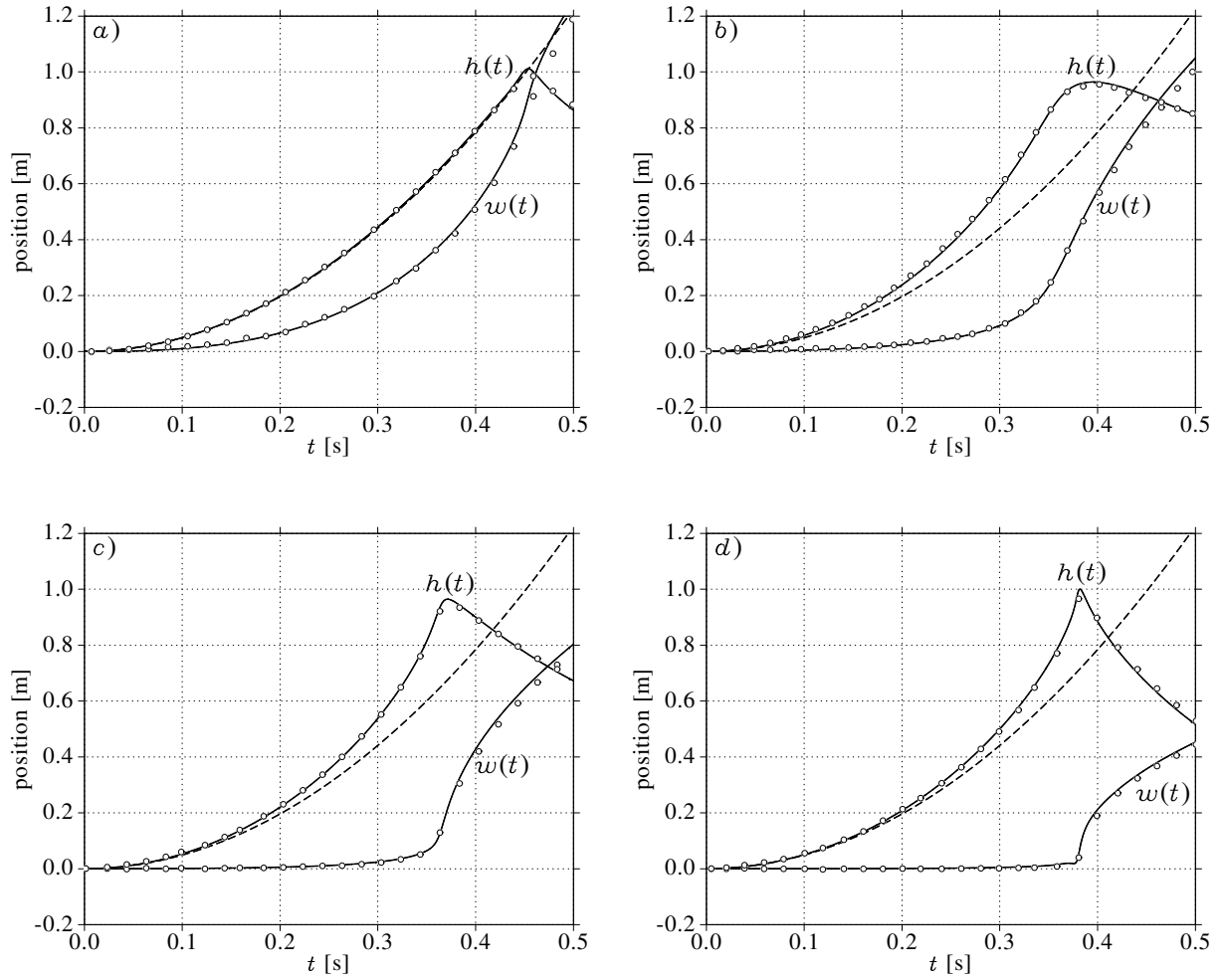


FIG. 5: The comparison of the vertical,  $h$ , and horizontal,  $w$ , fall distances of the falling chain tip found experimentally (circles) and numerically (solid lines). The parabola of the free fall is also shown (dotted lines). The initial separation between the chain ends is: a)  $x_0 = 1.0195$  m, b)  $x_0 = 0.765$  m, c)  $x_0 = 0.51$  m, and d)  $x_0 = 0.255$  m. Numerical data were obtained for  $r = 2.163 \cdot 10^{-5}$  Nms. The deviations between the numerical and experimental results are given in the central column of table I. See text.

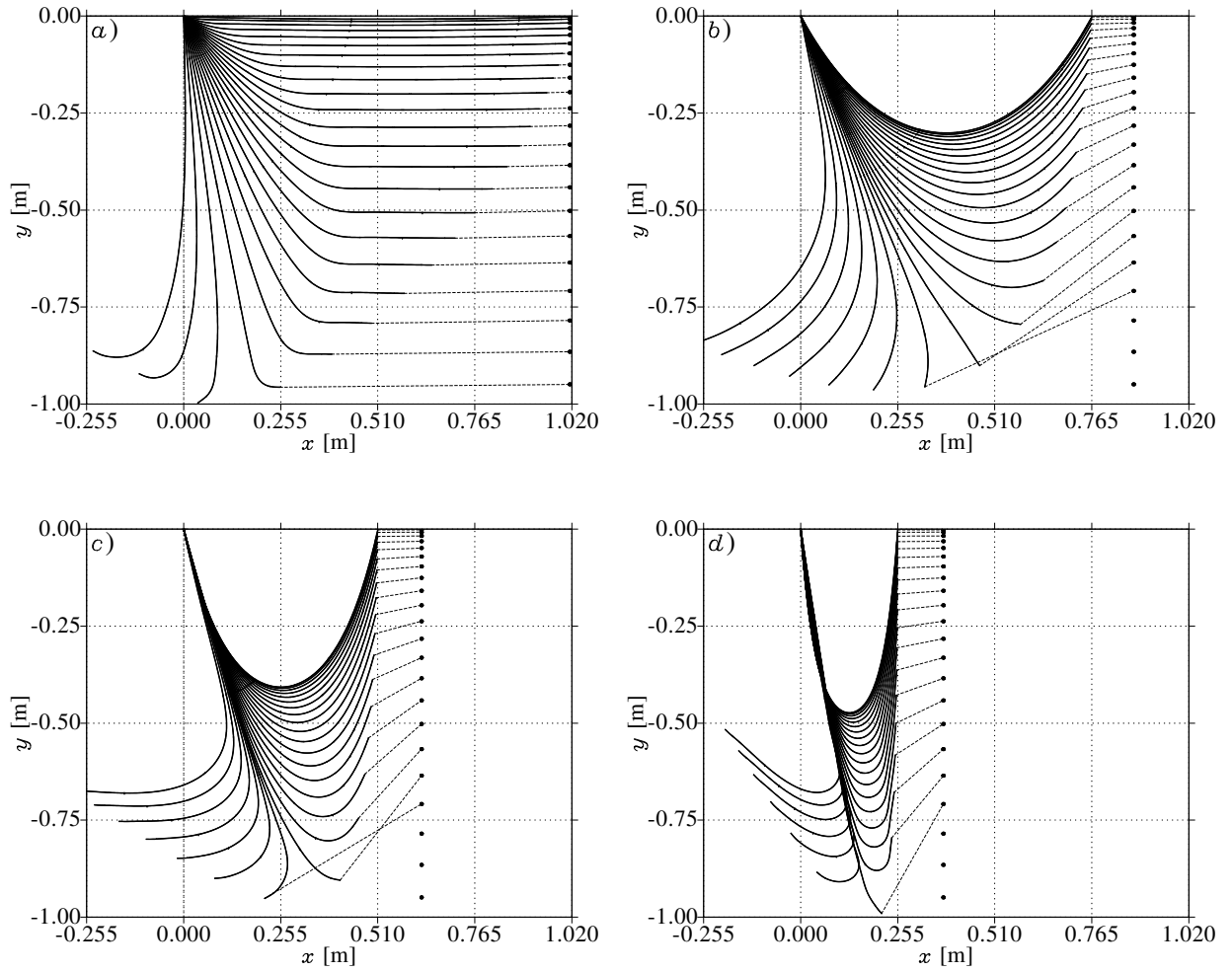


FIG. 6: Successive conformations of the falling chain vs. time found in numerical simulations. Simulations were performed with  $n = 229$ ,  $L = 1.02$  m,  $M = 0.0208$  kg,  $g = 9.81$  m/s<sup>2</sup> and the value of  $r = 2.163 \cdot 10^{-5}$  Nms, for which the numerical solutions of the equations of motion show a best fit to the results of the laboratory experiments. The initial conformations of the chain were discrete catenary curves with a)  $x_0 = 1.0195$  m, b)  $x_0 = 0.765$  m, c)  $x_0 = 0.51$  m and d)  $x_0 = 0.255$  m. Positions of the freely falling body are shown on the right hand sides of the figures; dotted lines connect them with the respective positions of the tip of the falling chain.

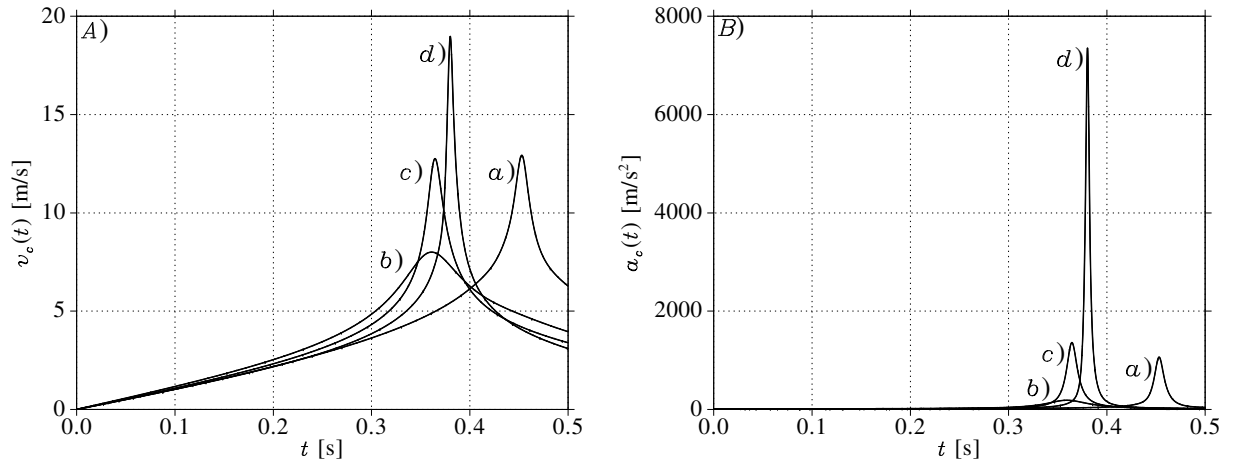


FIG. 7: Time evolution of the numerically determined moduli of the velocity and the acceleration of the falling chain tip. Initial separation of the chain ends: a)  $x_0 = 1.0195$  m, b)  $x_0 = 0.765$  m, c)  $x_0 = 0.51$  m, d)  $x_0 = 0.255$  m.  $r = 2.163 \cdot 10^{-5}$  Nms.

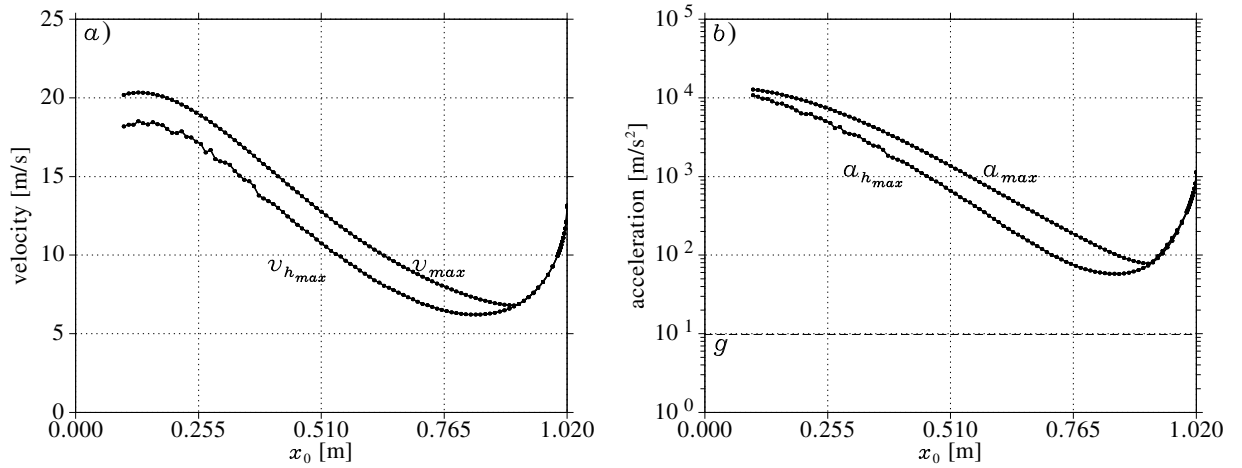


FIG. 8: Moduli of the velocity *a*) and acceleration *b*) of the chain tip versus the initial horizontal separation of the chain ends.  $v_{max}$  and  $a_{max}$  are, respectively, the maximum velocity and acceleration reached by the chain tip during its fall.  $v_{h_{max}}$  and  $a_{h_{max}}$  are the velocity and acceleration of the chain tip observed at the moment of time at which the tip reaches its lowest position. Picture *b* is plotted with a logarithmic scale. Gravitational acceleration  $g$  is marked with a dashed line. Plots presented in the figure were obtained numerically at  $r = 2.163 \cdot 10^{-5}$  Nms, for which the numerical solutions of the equations of motion best fit experimental results. See text.

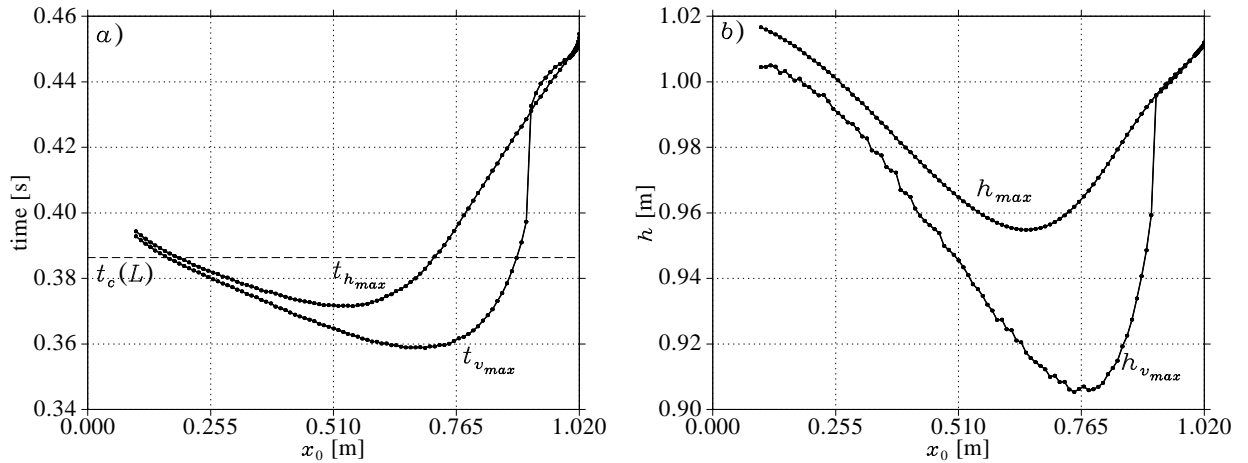


FIG. 9: *a)* Characteristic times,  $t_{h_{max}}$  and  $t_{v_{max}}$  versus initial separation  $x_0$ .  $t_{h_{max}}$  is the time at which the chain tip reaches its lowest position;  $t_{v_{max}}$  is the time at which it reaches its maximum velocity  $v_{max}$ . The dashed line represents the time  $t_c(L) \approx 0.386722$  at which the velocity diverges in the analytical model considered in section 2. *b)* Characteristic distances  $h_{max}$  and  $h_{v_{max}}$  versus initial separation  $x_0$ .  $h_{max}$  is the largest vertical fall distance reached by the chain tip;  $h_{v_{max}}$  is the vertical fall distance of the chain tip at which it reaches its maximum velocity. Plots presented in the figure were obtained numerically at  $r = 2.163 \cdot 10^{-5}$  Nms, for which the numerical solutions of the equations of motion fit best results of the laboratory experiments. See text.